EUROPEAN ORGANIZATION FOR NUCLEAR RESEARCH

CERN-PPE/92-164
22 September 1992

Search for Isosinglet Neutral Heavy Leptons in Z^0 Decays

The L3 Collaboration

Abstract

We search for neutral heavy leptons that are isosinglets under the Standard $SU(2)_L$ gauge group. Such neutral heavy leptons are expected in many extensions of the Standard Model. Three types of heavy leptons N_e, N_μ, N_τ associated with the three neutrino types ν_e, ν_μ, ν_τ have been directly searched for and no evidence for a signal has been found. We set the limit $Br(Z^0 \rightarrow \nu_\ell N_\ell) < 3 \times 10^{-5}$ at the 95% *C.L.* for the mass range from 3 GeV up to m_Z.

(Submitted to *Physics Letters B*)

1 Introduction

Isosinglet Neutral Heavy Leptons (INHL) arise in many models that attempt to unify the presently observed interactions into a single gauge scheme such as Grand Unified Theories or Superstring inspired models [1]. Their existence is also predicted in many extended electroweak models such as left-right symmetric and see-saw models [2].

Except the neutrinos, all the observed fundamental fermions that couple to the $SU(2)_L$ weak interaction have a right-handed component that transforms as an isosinglet. The simplest way to accommodate the lack of experimental evidence for right-handed neutrinos is to attribute it to an intrinsic asymmetry in the fermion spectrum, as in the Standard Model. This is made possible by the assumption that neutrinos are massless. However, there is no good theoretical basis for this choice [1, 3]. Small neutrino masses [3] can fit naturally in many theoretical contexts that include isosinglet neutral heavy leptons as right-handed neutrinos. Some models can also accomodate strictly massless light neutrinos, while keeping massive isosinglet partners [4].

Constraints on the isosinglet neutral lepton admixture in gauge currents have been placed by several experiments [5, 6]. The mass range covered, however, has been below 10 GeV, except for the limit obtained by the OPAL Collaboration which extends from 4 GeV up to m_{Z} [6].

In this paper we describe our search for an isosinglet neutral heavy lepton within the mass range from about 1 GeV up to m_{Z}. This search is based on the data collected at LEP with the L3 detector during 1990 and 1991 at centre of mass energies between 88.2 and 94.3 GeV. The total integrated luminosity is 17.5 pb^{-1}, corresponding to about 424,000 hadronic Z^0 decays.

2 The L3 detector

The L3 detector covers 99% of 4π. The detector consists of a central vertex chamber (TEC) with inner radius of 9 cm and outer of 47 cm, a high resolution electromagnetic calorimeter composed of BGO crystals extending from of 50 to 85 cm, a ring of scintillation counters, a uranium and brass hadron calorimeter with proportional wire chamber readout from 88 cm to 213 cm and a precise muon chamber system. These detectors are installed in a 12 m diameter magnet which provides a uniform field of 0.5 Tesla along the beam axis. The detector and its performance are described in detail elsewhere [7].

3 Production and decays

In this search, one isosinglet neutral heavy lepton N_ℓ is assumed to be associated with each generation of light neutrinos via the mixing amplitude U_ℓ. We do not consider mixing of the light neutrinos with higher isodoublet states (sequential leptons) nor the possibility of mixing among light neutrinos (as discussed in Ref. [4]). However, our results can be straightforwardly interpreted in such models. Also, the large mass difference between the light and heavy neutrinos allows us to ignore oscillation [4].

The mixing between the isosinglet neutral lepton and its associated isodoublet neutrino allows single production to occur in Z^0 decays[1]:

$$Z^0 \rightarrow N_\ell + \overline{\nu_\ell}$$

The production cross section is reduced from the neutrino pair production cross-section by a phase-space factor and by the square of a mixing amplitude. It can be written as [4, 8] :

$$\mathrm{Br}(Z^0 \rightarrow \nu_\ell N_\ell) = \mathrm{Br}(Z^0 \rightarrow \nu_\ell + \overline{\nu_\ell}) \, |U_\ell|^2 \, (1 - \frac{m_N^2}{m_Z^2})^2 \, (1 + \frac{1}{2}\frac{m_N^2}{m_Z^2})$$

where U_ℓ is the mixing amplitude, m_N the mass of N_ℓ and m_Z the mass of the Z^0. In contrast to Z^0 decay into sequential isodoublet neutral leptons where pair production is dominant (when kinematically allowed), here single production dominates because the corresponding pair production cross section is suppressed relatively to the single production cross section by an additional $|U_\ell|^2$ factor, which is expected to be small [8].

Isosinglet neutral leptons decay via the neutral or charged weak currents:

$$N_\ell \rightarrow Z^*\nu \text{ and } Z^* \rightarrow ee, \mu\mu, \tau\tau, \nu\nu, qq$$
$$N_\ell \rightarrow W^*\ell \text{ and } W^* \rightarrow e\nu, \mu\nu, \tau\nu, qq'$$

To calculate the branching ratios of these decays into the final states, we use the formulae from Refs. [4, 8]. For most of the mass range, the dominant decay mode is via charged currents, with a lepton and two quark final state, which is about 50% of the total rate. For low masses, the branching ratios depend on kinematical constraints, especially for the τ family, where for masses below 3 GeV, the dominant decay mode is via the neutral current with mainly a light neutrino and two quarks.

The mean decay length is a function of the coupling constant $|U_\ell|^2$ and the mass. It is given by [4]

$$L_N = \beta \, \gamma \, c \, \tau_N \;\propto\; \beta \, |U_\ell|^{-2} m_N^\alpha,$$

where $\alpha \approx -6$. This implies that the decay can occur far from the interaction point if the particle has a low mass or a very small coupling. We consider in our searches also the case where the decay occurs far from the interaction vertex (e.g. in the BGO calorimeter or in the hadron calorimeter), which allows us to consider mean decay lengths of up to 2 metres.

4 Monte-Carlo simulation

In order to determine the acceptance for detecting the isosinglet neutral lepton events, a Monte-Carlo generator based on the TIPTOP [9] and KORALZ [10] programs has been written. We include all mass effects and decay modes and assume the angular dependence for production to be $(1 + \cos^2\theta)$. For low mass studies, several mean decay lengths have been studied. Initial state radiation has been taken into account. For the decays involving quarks, we use JETSET with string fragmentation [11]. To estimate the background, we use various Monte-Carlo generators [10, 11, 12] to generate $Z^0 \rightarrow e^+e^-(\gamma)$, $\mu^+\mu^-(\gamma)$, $\tau^+\tau^-(\gamma)$ and $q\bar{q}(\gamma)$ decays.

[1] From here on, all arguments hold for particle as well as for antiparticle.

The Monte-Carlo events have been fully simulated in the L3 detector using the GEANT3 program [13], which takes into account the effects of energy loss, multiple scattering and showering in the materials, and then reconstructed in the same way as data.

5 Event signatures and selection

Because of the Lorentz boost in the laboratory frame, the decay signature depends on the mass of the isosinglet lepton. For low mass, we have mainly monojet events, while for high mass, two or more jets are dominant. The selection is subdivided according to the number of reconstructed jets. In this way, the efficiencies are optimized for all mass ranges in a natural manner. Jets are reconstructed based on the calorimeters information using the algorithm described in Ref. [14]. Isolated particles of at least 2 GeV with only one energy cluster in the BGO, such as electrons or muons, are considered as jets. A particle cluster from τ decay is also reconstructed as a single jet. In all searches, the electron identification relies on the shape of the energy deposition in the BGO calorimeter : the ratio of the energy deposited in a 3×3 crystal array ($\sum_9$) and a 5×5 array ($\sum_{25}$) must satisfy $\sum_9 / \sum_{25} > 0.95$, consistent with an electromagnetic shower shape. The muon identification is based on the reconstruction of a track in the muon chambers. This track is extrapolated backward towards the beam line and is required to pass within 100 mm from the interaction point in the $R-\phi$ plane and within 200 mm in the z direction. In the case of displaced vertex searches (see section 5.2), the tracks are required to pass within 400 mm from the interaction point in both the $R-\phi$ plane and the z direction.

The following trigger conditions are used for all the searches. The total energy trigger [15] requires a total energy of 15 GeV in the BGO and hadron calorimeter. The cluster trigger requires a cluster in the calorimeters with energy greater than 7 GeV. The charged cluster trigger requires a cluster in the calorimeter with an energy greater than 3 GeV and a TEC track pointing into the cluster direction. The single muon trigger selects events when at least one muon track with a transverse momentum with respect to the beam axis greater than 1.5 GeV is detected in the muon chambers and at least one scintillation counter has fired. The combined trigger efficiency is found to be close to 100% [16] in all decay modes for the events passing the cuts described below. From a study of inclusive muon events, the single muon trigger efficiency is found to be better than 95% for muons with energy greater than 5 GeV [17].

For the search for monojets with a displaced vertex, we cross-check the trigger efficiency by comparing it with the charged cluster trigger which has a lower energy threshold. The relative efficiency is found to exceed 99% for the events passing the cuts described below.

5.1 Search for monojets

By searching for monojet events, we cover inclusively all visible decay modes of an isosinglet lepton of mass ≤ 15 GeV. We select events that have exactly one reconstructed jet and at least two 'good' tracks[2)] in the TEC detector.

[2] A 'good' track is defined as having an impact parameter to the vertex smaller than 10 mm, at least 20 hits and a distance between the innermost and outermost used hit (in units of wire spacing) greater than 30 out of a maximum of 64. Its tranverse momentum must satisfy $P_t > 100$ MeV.

One source of background to this topology is $e^+e^- \rightarrow \tau^+\tau^-(\gamma)$ where the visible energy of one τ is below the threshold of the jet reconstruction algorithm due to the large fraction of energy carried away by the neutrino. In this case, however, some calorimetric energy and at least one low momentum track are expected in the hemisphere opposite to the monojet. We therefore require the energy in a cone of 30° half opening angle[3)] around the direction opposite to the jet to be less than 0.1 GeV and that no tracks exist in a 90° cone. The two distributions are shown in Fig. 1. The peak in the energy distribution centered at approximately 0.25 GeV corresponds to the energy deposition of minimum ionizing particles traversing the BGO calorimeter. The number of tracks in the 90° cone is computed without strict track quality requirement since we are interested in vetoing charged particles. The efficiency for reconstructing at least one track in the presence of a charged particle is calculated from Bhabha events and is $99.5 \pm 0.1\%$. The total number of events after the energy cut is 154 events, while we expect 137 ± 10 from Monte-Carlo. A small disagreement between the distributions of the data and Monte-Carlo is observed (see Fig. 1b). This is attributed to the splitting of tracks into two or more parts. This effect, which occurs only at low momentum, is underestimated in our simulation. This, however, does not affect our selection.

Two-photon process background events are produced dominantly at low polar angles and have small energy deposition. They are eliminated by requiring the energy of the monojet to be greater than 15 GeV and its polar angle to be in the range $20° < \theta < 160°$.

After applying all the cuts, we are left with 2 events from data, while we expect 0.6 ± 0.4 from $Z^0 \rightarrow \tau^+\tau^-(\gamma)$ events. One of the two candidates is shown in Fig. 2.

5.2 Search for monojets with a displaced vertex

As mentioned in section 3, low masses or small mixing amplitudes $|U_\ell|^2$ can result in decays far from the interaction point. To estimate the acceptance for such events, we generate all visible decay modes with decay lengths from a few cm up to 2 m. The detection efficiency can be parametrized as $\varepsilon_i \propto 1 - \exp(-L^i/L)$ where L^i is an effective length parameter depending on the decay mode i. The values of the L^i parameters for the various decay modes are shown in Table 1. From the monojet search with the track constraint (see section 5.1), we obtain $L^i = 30 \pm 1$ cm for all decay modes as the efficiency is dominated by the track quality requirement.

Without the track constraint, it is clear that the parameters L^i are larger for the decay modes for which selections are based on the hadron calorimeter and muon chambers, because of the larger decay distance between the production vertex and these subdetectors. For the $\nu\mu\mu$ decay mode, the effective parameter $L^{\nu\mu\mu}$ is dominated by the trigger efficiency.

For selecting monojet events, we use the cuts described in section 5.1 but remove the requirement on the number of 'good' TEC tracks. We restrict the searches to the barrel region of the detector. We apply further selection criteria based on the decay modes.

For purely electromagnetic monojets, we select the events with exactly one energy cluster with $\sum_9 / \sum_{25} > 0.95$ in the BGO calorimeter. We require that the energy deposited in the entire hadron calorimeter be less than 3 GeV, and that no energy is found in the luminosity monitor. The muon chambers must have no reconstructed segments in the three layers. To reduce background from the $e^+e^- \rightarrow \nu\bar{\nu}\gamma$ process, we require the energy of the cluster to be greater than 15 GeV. Applying the cuts to the data, we find one event while we expect 0.6 ± 0.6 events from the $e^+e^- \rightarrow \nu\bar{\nu}\gamma$ process. The candidate has a cluster of 19 GeV with no activity in the rest of the detector.

[3] All the cone sizes mentioned refer to the half opening angle of the cone.

Decay mode i	L^i (cm)
$\mathrm{N} \to \mathrm{e}\mathrm{q}\overline{\mathrm{q}}$	81 $\pm$ 7
$\mathrm{N} \to \mu\mathrm{q}\overline{\mathrm{q}}$	120 $\pm$ 10
$\mathrm{N} \to \tau\mathrm{q}\overline{\mathrm{q}}$	81 $\pm$ 7
$\mathrm{N} \to \nu\mathrm{e}\overline{\mathrm{e}}$	56 $\pm$ 6
$\mathrm{N} \to \nu\mu\overline{\mu}$	33 $\pm$ 3
$\mathrm{N} \to \nu\tau\overline{\tau}$	61 $\pm$ 4
$\mathrm{N} \to \nu\mathrm{e}\overline{\mu}$	88 $\pm$ 7
$\mathrm{N} \to \nu\mathrm{e}\overline{\tau}$	81 $\pm$ 7
$\mathrm{N} \to \nu\mu\overline{\tau}$	88 $\pm$ 7
$\mathrm{N} \to \nu\mathrm{q}\overline{\mathrm{q}}$	81 $\pm$ 7

Table 1: Fitted values of the L^i parameter of the parametrization of the dependence of the acceptance with displaced vertex for different decay modes.

For monojets with electromagnetic and hadronic activity, we require the energy deposited in the BGO calorimeter to be at least 2 GeV and the energy in the hadronic calorimeter to be at least 5 GeV. The total energy should be greater than 15 GeV. The muon chambers must have no reconstructed segments in the three layers. To remove contamination from cosmic rays, we ask for at least one scintillator hit within ± 1.5 ns of the beam crossing. We find no candidates for this mode.

For events with mostly hadronic activity, the energy of the jet must be at least 20 GeV and there should be less than 2 GeV deposited in the BGO calorimeter. To remove cosmic rays, we ask for at least one scintillator hit in time. We apply a cut on the lateral and longitudinal shape of the shower development so that it is compatible with particles coming from the interaction point. This removes the background originating from the beam halo, produced by particles entering horizontally through the sides of the hadron calorimeter. Only one event survives the selection.

We also search for monojets containing at least one muon. We find no candidates for this decay mode.

5.3 Search for two acoplanar jets

This event topology consists of a pair of acoplanar and acollinear jets with large missing energy and transverse imbalance. This search covers all decay modes containing a neutrino in the final state for the mass region $\geq$ 15 GeV and the modes containing hadrons and a lepton for the mass region 15 GeV $\leq m_{\mathrm{N}} \leq$ 50 GeV. Backgrounds to this topology come from events where some energy is either unseen or not well measured in the detector.

We select all events which have exactly two reconstructed jets and at least two 'good' tracks. Almost all dilepton and hadronic decays of the Z^0 are removed by requiring an acollinearity η between the two jets greater than 35° and an acoplanarity $\delta\phi$ greater than 20°. The distributions of η and $\delta\phi$ are shown in Fig. 3.

Initial state radiation and two-photon background are reduced by the requirement that the polar angle θ_m of the missing momentum should satisfy $20° < \theta_m < 160°$. The most energetic jet must have at least 10 GeV and the second jet at least 5 GeV. Remaining background is removed by requiring that the energy in the 30° cone around the direction of the missing momentum be less than 0.2 GeV and that the number of tracks in this cone be zero.

After applying all cuts, one event is left in the data while we expect 0.2 ± 0.2 from the $Z^0 \to \tau^+\tau^-(\gamma)$ decay. The candidate is shown in Fig. 4.

5.4 Search for isolated leptons in three or more jets

By selecting hadronic events with an isolated lepton, we search for the ℓqq decay modes for the mass region ≥ 50 GeV.

The main background to this topology comes from the semileptonic decays of heavy quarks. Radiative hadronic decays $Z^0 \to q\bar{q}\gamma$ where a hard photon converts in the beam-pipe can also fake an isolated electron.

We select events with three or more reconstructed jets. The visible energy must be greater than $0.4\sqrt{s}$. The energy of the third jet must be at least 5 GeV, to remove the QCD background. For the eqq mode, there must be an electromagnetic cluster of at least 5 GeV with $\sum_9 / \sum_{25} > 0.95$ and a TEC track within $\pm$ 10 mrad in the r-ϕ plane. The isolation criterium is that the energy in the 30° cone around the electron candidate is less than 3 GeV. For the μqq mode, the energy in the 30° around the muon must be less than 5 GeV (in this case, we do not subtract the calorimetric energy loss of the muon). To improve the rejection of hadronic background where a jet is mismeasured, we require that the energy in a 20° cone around the missing momentum direction be less than 2 GeV. This cut is applied only when the visible energy is less than $0.9\sqrt{s}$, i.e. when the direction of missing momentum is well defined. In the τqq mode, the identification of an isolated tau suffers from the large background from hadronic events. We look for isolated tracks with momentum greater than 2 GeV. There should not be any other track inside the 20° cone around this track. The energy inside the 10° cone around the track should be more than 3 GeV, and the difference of energies in the 20° and 10° cones around the track should be less than 1 GeV. The acoplanarity between the two most energetic jets has to be greater than 30°.

After applying our selection cuts to the data, we find a total of 42 candidates in the three decay modes. The data events and the Monte-Carlo background expectations are shown in Table 2.

Decay Mode	Data	Monte-Carlo
eqq	6	7 ± 2
μqq	10	7 ± 2
τqq	26	23 ± 3

Table 2: List of selected events in data and Monte-Carlo.

In these decay modes, the reconstruction of the invariant mass of the isosinglet neutral lepton is possible due to the presence of only one light neutrino in the final state. The reconstructed masses have a resolution of 11% for the eqq and μqq modes and 15% for the τqq mode. We rescale the invariant mass as follows:

$$m_N^{corr} = m_N \frac{\sqrt{s}}{p_\nu + E}$$

where p_ν is the missing momentum of the event, and E is the event energy. This improves the resolution on the mass measurement to 6% for the eqq and μqq modes and 11% for the τqq mode almost independently of the mass. The invariant mass distributions for data and background Monte-Carlo are shown in Fig. 5. The selected events are grouped in the mass region $\approx$ 80-90 GeV. These events are compatible with the expected background.

6 Results

We calculate the 95% confidence level upper limit on the square of the mixing amplitude and the branching ratio for each generation. Following Ref. [19], the probability ϵ for observing in different channels j ($j = 1, .., J_c$) J_j events or less for a signal s and estimated background b_j is given by

$$\epsilon = \prod_{j=1}^{J_c} \left(\sum_{n=0}^{J_j} \int g_j(b) P(n; \varepsilon_j s + b) \mathrm{d}b \right) / \left(\sum_{n_b=0}^{J_j} \int g_j(b) P(n_b; b) \mathrm{d}b \right)$$

where ε_j is defined as

$$\varepsilon_j = \sum_i \varepsilon_j^i r_i$$

where the summation is made over the decay modes i. P is the Poisson distribution function. ε_j^i is the detection efficiency for the decay mode i in the channel j. r_i is the branching ratio of this decay mode. $g_j(b)$ is the probability distribution for the background in the channel j, which is assumed to follow a Poisson distribution of mean b_j.

The list of channels along with the data candidates and Monte-Carlo background events are shown in Table 3. For the case with three or more jets, the number of events in data and Monte-Carlo background for a given mass M is defined as the number of events which have a reconstructed mass in the range of $\mathrm{M} \pm 1.5\sigma_M$, where σ_M varies from 3 to 8 GeV for different masses and decay modes.

Channel	Data	Monte-Carlo
Purely electromagnetic monojet without TEC tracks	1	0.6±0.6
Purely hadronic monojet without TEC tracks	1	0
Monojet with TEC tracks and without muon tracks	2	0.6±0.4
Monojet with muon tracks	0	0
Two jet events	1	0.2±0.2
Three or more jets events	see text	

Table 3: List of channels used for the determination of the limits.

The combined efficiencies for the various decay modes are listed in Table 4. The efficiencies are all above 20%, expect in the τqq mode where the efficiency drops for masses very close to m_{Z}. The sources of systematic errors in the determination of the upper limits are the following:

- 2% absolute systematical uncertainties in the Monte-Carlo simulation of the detector;
- 2% statistical error in the determination of the signal detection efficiencies due to limited Monte Carlo statistics;
- 0.5% experimental uncertainty on the number of hadronic events [18].

The results for the mixing coupling constant as a function of the mass is shown in Fig. 6. The mixing term $|U_\ell|^2$ is constrained to be less than 2×10^{-4} for the mass range $3 < \mathrm{m_N} < 50$ GeV. Above 50 GeV, the limit worsens due to the phase space factor. In terms of branching ratio, the limit can be expressed as $\mathrm{Br}(\mathrm{Z}^0 \to \nu_\ell \mathrm{N}_\ell) < 3 \times 10^{-5}$ for masses from 3 GeV up to m_{Z}. The coupling constant limit as a function of the mean decay length L is shown in Fig. 7.

Mass (GeV)	5	30	50	68	78	89
$N \to e q\overline{q}$	48	44	47	49	40	22
$N \to \mu q\overline{q}$	49	42	35	34	39	32
$N \to \tau q\overline{q}$	50	40	35	33	10	3
$N \to \nu e\overline{e}$	54	49	56	44	36	37
$N \to \nu \mu\overline{\mu}$	42	42	39	36	39	30
$N \to \nu \tau\overline{\tau}$	36	23	24	20	22	20
$N \to \nu e\overline{\mu}$	47	43	41	45	50	45
$N \to \nu e\overline{\tau}$	31	34	38	38	40	38
$N \to \nu \mu\overline{\tau}$	30	36	34	36	37	35
$N \to \nu q\overline{q}$	37	38	43	42	32	26

Table 4: Detection efficiency in percent for different INHL masses and decay modes.

7 Conclusion

We searched for all visible decay modes of an isosinglet neutral lepton from very low masses up to m_Z. We also searched for displaced vertex decays. No excess was found in the data. We set limits of the order of 10^{-4} on the mixing term $|U_\ell|^2$ as a function of the mass and as a function of the decay length. These correspond to limits of the order of 3×10^{-5} on the branching ratio $\mathrm{Br}(Z^0 \to \nu_\ell N_\ell)$.

Acknowledgments

We wish to express our gratitude to the CERN accelerator divisions for the excellent performance of the LEP machine. We acknowledge the efforts of all engineers and technicians who have participated in the construction and maintenance of this experiment.

The L3 Collaboration:

O.Adriani,[14] M.Aguilar-Benitez,[23] S.Ahlen,[9] J.Alcaraz,[15] A.Aloisio,[26] G.Alverson,[10] M.G.Alviggi,[26] G.Ambrosi,[31] Q.An,[16] H.Anderhub,[45] A.L.Anderson,[13] V.P.Andreev,[35] T.Angelov,[13] L.Antonov,[39] D.Antreasyan,[7] P.Arce,[23] A.Arefiev,[25] A.Atamanchuk,[35] T.Azemoon,[3] T.Aziz,[8,1] P.V.K.S.Baba,[16] P.Bagnaia,[34] J.A.Bakken,[33] L.Baksay,[41] R.C.Ball,[3] S.Banerjee,[8] J.Bao,[5] R.Barillère,[15] L.Barone,[34] A.Baschirotto,[24] R.Battiston,[31] A.Bay,[17] F.Becattini,[14] U.Becker,[13,45] F.Behner,[45] J.Behrens,[45] S.Beingessner,[4] Gy.L.Bencze,[11] J.Berdugo,[23] P.Berges,[13] B.Bertucci,[31] B.L.Betev,[39,45] M.Biasini,[31] A.Biland,[45] G.M.Bilei,[31] R.Bizzarri,[34] J.J.Blaising,[4] G.J.Bobbink,[15,2] M.Bocciolini,[14] R.Bock,[1] A.Böhm,[1] B.Borgia,[34] M.Boseti,[24] D.Bourilkov,[28] M.Bourquin,[17] D.Boutigny,[4] B.Bouwens,[2] E.Brambilla,[26] J.G.Branson,[36] I.C.Brock,[32] M.Brooks,[21] C.Buisson,[22] A.Bujak,[42] J.D.Burger,[13] W.J.Burger,[17] J.Busenitz,[41] X.D.Cai,[16] M.Capell,[20] M.Caria,[31] G.Carlino,[26] F.Carminati,[14] A.M.Cartacci,[14] R.Castello,[24] M.Cerrada,[23] F.Cesaroni,[34] Y.H.Chang,[13] U.K.Chaturvedi,[16] M.Chemarin,[22] A.Chen,[47] C.Chen,[6] G.M.Chen,[6] H.F.Chen,[18] H.S.Chen,[6] J.Chen,[13] M.Chen,[13] M.L.Chen,[3] W.Y.Chen,[16] G.Chiefari,[26] C.Y.Chien,[5] M.Chmeissani,[3] M.T.Choi,[40] S.Chung,[13] C.Civinini,[14] I.Clare,[13] R.Clare,[13] T.E.Coan,[21] H.O.Cohn,[29] G.Coignet,[4] N.Colino,[15] A.Contin,[7] F.Crijns,[28] X.T.Cui,[16] X.Y.Cui,[16] T.S.Dai,[13] R.D'Alessandro,[14] R.de Asmundis,[26] A.Degré,[4] K.Deiters,[13] E.Dénes,[11] P.Denes,[33] F.DeNotaristefani,[34] M.Dhina,[45] D.DiBitonto,[41] M.Diemoz,[34] H.R.Dimitrov,[39] C.Dionisi,[34,15] M.T.Dova,[16] E.Drago,[26] T.Driever,[28] D.Duchesneau,[17] P.Duinker,[2] I.Duran,[37] S.Easo,[31] H.El Mamouni,[22] A.Engler,[32] F.J.Eppling,[13] F.C.Erné,[2] P.Extermann,[17] R.Fabbretti,[43] M.Fabre,[43] S.Falciano,[34] S.J.Fan,[38] O.Fackler,[20] J.Fay,[22] M.Felcini,[15] T.Ferguson,[32] D.Fernandez,[23] G.Fernandez,[23] F.Ferroni,[34] H.Fesefeldt,[1] E.Fiandrini,[31] J.Field,[17] F.Filthaut,[28] G.Finocchiaro,[34] P.H.Fisher,[5] G.Forconi,[17] T.Foreman,[2] K.Freudenreich,[45] W.Friebel,[44] M.Fukushima,[13] M.Gailloud,[19] Yu.Galaktionov,[25,13] E.Gallo,[14] S.N.Ganguli,[15,8] P.Garcia-Abia,[23] S.S.Gau,[47] D.Gele,[22] S.Gentile,[34,15] S.Goldfarb,[10] Z.F.Gong,[18] E.Gonzalez,[23] P.Göttlicher,[1] A.Gougas,[5] D.Goujon,[17] G.Gratta,[30] C.Grinnell,[13] M.Gruenewald,[30] C.Gu,[16] M.Guanziroli,[16] J.K.Guo,[38] V.K.Gupta,[33] A.Gurtu,[8] H.R.Gustafson,[3] L.J.Gutay,[42] K.Hangarter,[1] A.Hasan,[16] D.Hauschildt,[2] C.F.He,[38] T.Hebbeker,[1] M.Hebert,[36] G.Herten,[13] U.Herten,[1] A.Hervé,[15] K.Hilgers,[1] H.Hofer,[45] H.Hoorani,[17] G.Hu,[16] G.Q.Hu,[38] B.Ille,[22] M.M.Ilyas,[16] V.Innocente,[15] H.Janssen,[15] S. Jezequel,[4] B.N.Jin,[6] L.W.Jones,[3] A.Kasser,[19] R.A.Khan,[16] Yu.Kamyshkov,[29] P.Kapinos,[35,44] J.S.Kapustinsky,[21] Y.Karyotakis,[15] M.Kaur,[16] S.Khokhar,[16] M.N.Kienzle-Focacci,[17] J.K.Kim,[40] S.C.Kim,[40] Y.G.Kim,[40] W.W.Kinnison,[21] D.Kirkby,[30] S.Kirsch,[44] W.Kittel,[28] A.Klimentov,[13,25] A.C.König,[28] E.Koffeman,[2] O.Kornadt,[1] V.Koutsenko,[13,25] A.Koulbardis,[35] R.W.Kraemer,[32] T.Kramer,[13] V.R.Krastev,[39,31] W.Krenz,[1] A.Krivshich,[35] H.Kuijten,[28] K.S.Kumar,[12] A.Kunin,[12,25] G.Landi,[14] D.Lanske,[1] S.Lanzano,[26] P.Lebrun,[22] P.Lecomte,[45] P.Lecoq,[15] P.Le Coultre,[45] D.M.Lee,[21] I.Leedom,[10] J.M.Le Goff,[15] R.Leiste,[44] M.Lenti,[14] E.Leonardi,[34] J.Lettry,[45] X.Leytens,[2] C.Li,[18,16] H.T.Li,[6] P.J.Li,[38] X.G.Li,[6] J.Y.Liao,[38] W.T.Lin,[47] Z.Y.Lin,[18] F.L.Linde,[15] B.Lindemann,[1] D.Linnhofer,[45] L.Lista,[26] Y.Liu,[16] W.Lohmann,[44,15] E.Longo,[34] Y.S.Lu,[6] J.M.Lubbers,[15] K.Lübelsmeyer,[1] C.Luci,[34] D.Luckey,[7,13] L.Ludovici,[34] L.Luminari,[34] W.Lustermann,[44] J.M.Ma,[6] W.G.Ma,[18] M.MacDermott,[45] P.K.Malhotra,[8]† R.Malik,[16] A.Malinin,[4,25] C.Maña,[23] D.N.Mao,[3] Y.F.Mao,[6] M.Maolinbay,[45] P.Marchesini,[45] F.Marion,[4] A.Marin,[9] J.P.Martin,[22] L.Martinez-Laso,[23] F.Marzano,[34] G.G.G.Massaro,[2] T.Matsuda,[13] K.Mazumdar,[8] P.McBride,[12] T.McMahon,[42] D.McNally,[45] M.Merk,[28] L.Merola,[26] M.Meschini,[14] W.J.Metzger,[28] Y.Mi,[19] G.B.Mills,[21] Y.Mir,[16] G.Mirabelli,[34] J.Mnich,[1] M.Möller,[1] B.Monteleoni,[14] R.Morand,[4] S.Morganti,[34] N.E.Moulai,[16] R.Mount,[30] S.Müller,[1] A.Nadtochy,[35] E.Nagy,[11] M.Napolitano,[26] H.Newman,[30] C.Neyer,[45] M.A.Niaz,[16] A.Nippe,[1] H.Nowak,[44] G.Organtini,[34] D.Pandoulas,[1] S.Paoletti,[14] P.Paolucci,[26] G.Passaleva,[14,31] S.Patricelli,[26] T.Paul,[5] M.Pauluzzi,[31] F.Pauss,[45] Y.J.Pei,[1] S.Pensotti,[24] D.Perret-Gallix,[4] J.Perrier,[17] A.Pevsner,[5] D.Piccolo,[26] M.Pieri,[15] P.A.Piroué,[33] F.Plasil,[29] V.Plyaskin,[25] M.Pohl,[45] V.Pojidaev,[25,14] N.Produit,[17] J.M.Qian,[3] K.N.Qureshi,[16] R.Raghavan,[8] G.Rahal-Callot,[45] P.G.Rancoita,[24] M.Rattaggi,[24] G.Raven,[2] P.Razis,[27] K.Read,[29] D.Ren,[45] Z.Ren,[16] M.Rescigno,[34] S.Reucroft,[10] A.Ricker,[1] S.Riemann,[44] W.Riemers,[42] K.Riles,[3] O.Rind,[3] H.A.Rizvi,[16] F.J.Rodriguez,[23] B.P.Roe,[3] M.Röhner,[1] S.Röhner,[1] L.Romero,[23] J.Rose,[1] S.Rosier-Lees,[4] R.Rosmalen,[28] Ph.Rosselet,[19] A.Rubbia,[13] J.A.Rubio,[15] H.Rykaczewski,[45] M.Sachwitz,[44] E.Sajan,[31] J.Salicio,[15] J.M.Salicio,[23] G.S.Sanders,[21] A.Santocchia,[31] M.S.Sarakinos,[13] G.Sartorelli,[7,16] M.Sassowsky,[1] G.Sauvage,[4] V.Schegelsky,[35] D.Schmitz,[1] P.Schmitz,[1] M.Schneegans,[4] H.Schopper,[46] D.J.Schotanus,[28] S.Shotkin,[13] H.J.Schreiber,[44] J.Shukla,[32] R.Schulte,[1] S.Schulte,[1] K.Schultze,[1] J.Schwenke,[1] G.Schwering,[1] C.Sciacca,[26] I.Scott,[12] R.Sehgal,[16] P.G.Seiler,[43] J.C.Sens,[15,2] L.Servoli,[31] I.Sheer,[36] D.Z.Shen,[38] S.Shevchenko,[30] X.R.Shi,[30] E.Shumilov,[25] V.Shoutko,[25] E.Soderstrom,[33] D.Son,[40] A.Sopczak,[36] C.Spartiotis,[5] T.Spickermann,[1] P.Spillantini,[14] R.Starosta,[1] M.Steuer,[7,13] D.P.Stickland,[33] F.Sticozzi,[13] H.Stone,[17] K.Strauch,[12] B.C.Stringfellow,[42] K.Sudhakar,[8] G.Sultanov,[16] R.L.Sumner,[33] L.Z.Sun,[18,16] H.Suter,[45] R.B.Sutton,[32] J.D.Swain,[16] A.A.Syed,[16] X.W.Tang,[6] L.Taylor,[10] G.Terzi,[24] C.Timmermans,[28] Samuel C.C.Ting,[13] S.M.Ting,[13] M.Tonutti,[1] S.C.Tonwar,[8] J.Tóth,[11] A.Tsaregorodtsev,[35] G.Tsipolitis,[32] C.Tully,[30] K.L.Tung,[6] J.Ulbricht,[45] L.Urbán,[11] U.Uwer,[1] E.Valente,[34] R.T.Van de Walle,[28] I.Vetlitsky,[25] G.Viertel,[45] P.Vikas,[16] U.Vikas,[16] M.Vivargent,[4] H.Vogel,[32] H.Vogt,[44] I.Vorobiev,[25] A.A.Vorobyov,[35] L.Vuilleumier,[19] M.Wadhwa,[16] W.Wallraff,[1] C.R.Wang,[18] G.H.Wang,[32] J.H.Wang,[6] X.L.Wang,[18] Y.F.Wang,[13] Z.M.Wang,[16,18] A.Weber,[1] J.Weber,[45] R.Weill,[19] T.J.Wenaus,[20] J.Wenninger,[17] M.White,[13] C.Willmott,[23] F.Wittgenstein,[15] D.Wright,[33] R.J.Wu,[6] S.X.Wu,[16] Y.G.Wu,[6] B.Wysłouch,[13] Y.Y.Xie,[38] Y.D.Xu,[6] Z.Z.Xu,[18] Z.L.Xue,[38] D.S.Yan,[38] X.J.Yan,[13] B.Z.Yang,[18] C.G.Yang,[6] G.Yang,[16] K.S.Yang,[6] Q.Y.Yang,[6] Z.Q.Yang,[38] C.H.Ye,[16] J.B.Ye,[18] Q.Ye,[16] S.C.Yeh,[47] Z.W.Yin,[38] J.M.You,[16] N.Yunus,[16] M.Yzerman,[2] C.Zaccardelli,[30] P.Zemp,[45] M.Zeng,[16] Y.Zeng,[1] D.H.Zhang,[2] Z.P.Zhang,[18,16] B.Zhou,[9] J.F.Zhou,[1] R.Y.Zhu,[30] H.L.Zhuang,[6] A.Zichichi,[7,15,16] B.C.C.van der Zwaan.[2]

1 I. Physikalisches Institut, RWTH, W-5100 Aachen, FRG[§]
III. Physikalisches Institut, RWTH, W-5100 Aachen, FRG[§]
2 National Institute for High Energy Physics, NIKHEF, NL-1009 DB Amsterdam, The Netherlands
3 University of Michigan, Ann Arbor, MI 48109, USA
4 Laboratoire d'Annecy-le-Vieux de Physique des Particules, LAPP,IN2P3-CNRS, BP 110, F-74941 Annecy-le-Vieux CEDEX, France
5 Johns Hopkins University, Baltimore, MD 21218, USA
6 Institute of High Energy Physics, IHEP, Beijing, China
7 INFN-Sezione di Bologna, I-40126 Bologna, Italy
8 Tata Institute of Fundamental Research, Bombay 400 005, India
9 Boston University, Boston, MA 02215, USA
10 Northeastern University, Boston, MA 02115, USA
11 Central Research Institute for Physics of the Hungarian Academy of Sciences, H-1525 Budapest 114, Hungary[‡]
12 Harvard University, Cambridge, MA 02139, USA
13 Massachusetts Institute of Technology, Cambridge, MA 02139, USA
14 INFN Sezione di Firenze and University of Florence, I-50125 Florence, Italy
15 European Laboratory for Particle Physics, CERN, CH-1211 Geneva 23, Switzerland
16 World Laboratory, FBLJA Project, CH-1211 Geneva 23, Switzerland
17 University of Geneva, CH-1211 Geneva 4, Switzerland
18 Chinese University of Science and Technology, USTC, Hefei, Anhui 230 029, China
19 University of Lausanne, CH-1015 Lausanne, Switzerland
20 Lawrence Livermore National Laboratory, Livermore, CA 94550, USA
21 Los Alamos National Laboratory, Los Alamos, NM 87544, USA
22 Institut de Physique Nucléaire de Lyon, IN2P3-CNRS,Université Claude Bernard, F-69622 Villeurbanne Cedex, France
23 Centro de Investigaciones Energeticas, Medioambientales y Tecnologicas, CIEMAT, E-28040 Madrid, Spain
24 INFN-Sezione di Milano, I-20133 Milan, Italy
25 Institute of Theoretical and Experimental Physics, ITEP, Moscow, Russia
26 INFN-Sezione di Napoli and University of Naples, I-80125 Naples, Italy
27 Department of Natural Sciences, University of Cyprus, Nicosia, Cyprus
28 University of Nymegen and NIKHEF, NL-6525 ED Nymegen, The Netherlands
29 Oak Ridge National Laboratory, Oak Ridge, TN 37831, USA
30 California Institute of Technology, Pasadena, CA 91125, USA
31 INFN-Sezione di Perugia and Universitá Degli Studi di Perugia, I-06100 Perugia, Italy
32 Carnegie Mellon University, Pittsburgh, PA 15213, USA
33 Princeton University, Princeton, NJ 08544, USA
34 INFN-Sezione di Roma and University of Rome, "La Sapienza", I-00185 Rome, Italy
35 Nuclear Physics Institute, St. Petersburg, Russia
36 University of California, San Diego, CA 92182, USA
37 Dept. de Fisica de Particulas Elementales, Univ. de Santiago, E-15706 Santiago de Compostela, Spain
38 Shanghai Institute of Ceramics, SIC, Shanghai, China
39 Bulgarian Academy of Sciences, Institute of Mechatronics, BU-1113 Sofia, Bulgaria
40 Center for High Energy Physics, Korea Advanced Inst. of Sciences and Technology, 305-701 Taejon, Republic of Korea
41 University of Alabama, Tuscaloosa, AL 35486, USA
42 Purdue University, West Lafayette, IN 47907, USA
43 Paul Scherrer Institut, PSI, CH-5232 Villigen, Switzerland
44 DESY-Institut für Hochenergiephysik, O-1615 Zeuthen, FRG
45 Eidgenössische Technische Hochschule, ETH Zürich, CH-8093 Zürich, Switzerland
46 University of Hamburg, W-2000 Hamburg, FRG
47 High Energy Physics Group, Taiwan, China

§ Supported by the German Bundesministerium für Forschung und Technologie
‡ Supported by the Hungarian OTKA fund under contract number 2970.

† Deceased.

References

[1] For a review, see J.W.F. Valle, in Weak and electromagnetic interactions in nuclei, eds. H. Klapdor (Springer, Berlin, 1968) p. 927.

[2] M. Gell-Mann, P. Ramond, R. Slansky in Supergravity, eds. by D. Freedman *et al.*, (North Holland, 1979);
T. Yanagida, KEK lectures, eds. O. Sawada *et al.* (1979);
R. Mohaparta, G. Senjanovic, Phys. Rev. Lett. **44** (1980) 912, Phys. Rev. **D23** (1981) 165.

[3] For a recent review, see J.W.F. Valle, Nucl. Phys. (Proc. Suppl) **11** (1989) p.118.

[4] M. Gronau, C. Leung and J. Rosner, Phys. Rev. **D29** (1984) 2539.

[5] G. J. Feldman *et al.*, Phys. Rev. Lett. **54** (1985) 2289.
A. M. Cooper-Sarkar *et al.*, Phys. Lett. **160B** (1985) 207.
J. Dorenbosch *et al.*, Phys. Lett. **166B** (1986) 473 and references therein.
S. R. Mishra *et al.*, Phys. Rev. Lett. **59** (1987) 1397.
M. E. Duffy *et al.*, Phys. Rev. **D38** (1988) 2032.
W. Bartel *et al.*, Phys. Lett. **123B** (1983) 353.
CCFR Collaboration, K. Bachmann *et al.*, Preprint **UR-1157**.

[6] OPAL Collaboration, M. Z. Akrawy et. al., Phys. Lett. **247B** (1990) 448.

[7] L3 Collaboration, B. Adeva *et al.*, Nucl. Instr. and Meth. **A289** (1990) 35.

[8] M. Dittmar, M.C. Gonzalez-Garcia, A. Santamaria and J.W.F. Valle, Nucl. Phys. **B332** (1990) 1.

[9] S. Jadach and J. Kühn, TIPTOP Monte Carlo, preprint MPI-PAE/PTh 64/86.

[10] S. Jadach *et al.*, "Z Physics at LEP 1", eds. G. Altarelli *et al.*, CERN Report CERN-89-08, Vol. 3 (1989) 69.

[11] T. Sjöstrand and M. Bengtsson, Comput. Phys. Commun. **43** (1987) 367;
T. Sjöstrand, "Z Physics at LEP 1", eds. G. Altarelli *et al.*, CERN Report CERN-89-08, Vol. 3 (1989) 143.

[12] M. Böhm, A. Denner and W. Hollik, Nucl. Phys. **B304** (1988) 687;
F.A. Berends, R. Kleiss and W. Hollik, Nucl. Phys. **B304** (1988) 712.

[13] GEANT Version 3.13, September, 1989. See R. Brun *et al.*, "GEANT 3", CERN DD/EE/84-1 (Revised), Sept. 1987; The GHEISHA program is used to simulate hadronic interactions. See H. Fesefeldt, RWTH Aachen Report PITHA 85/02 (1985).

[14] O. Adriani *et al.*, Nucl. Instr. and Meth. **A302** (1991) 53.

[15] R. Bizzarri *et al.*, Nucl. Instr. and Meth. **A283** (1989) 799.

[16] L3 Collab., B. Adeva *et al.*, Phys. Lett. **B248** (1990) 203.

[17] L3 Collab., B. Adeva *et al.*, Phys. Lett. **B252** (1990) 703.

[18] L3 Collab., B. Adeva *et al.*, Z Phys. **C51** (1991) 1179.

[19] G. Zech, Nucl. Instr. and Meth. **A277** (1989) 608;
O. Helene, Nucl. Instr. and Meth. **A212** (1983) 319.

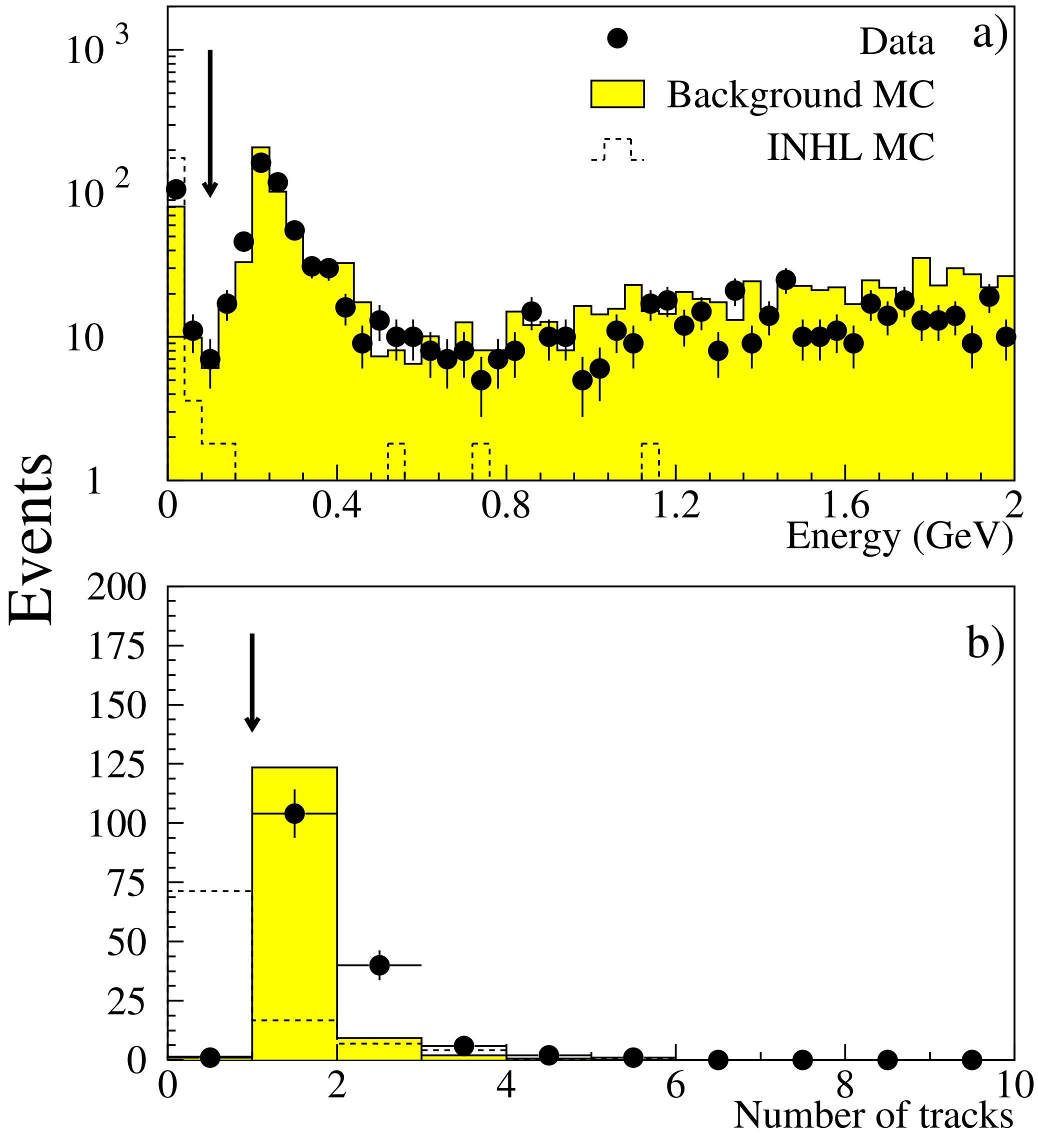

Figure 1: a) Energy in the 30° cone around the opposite direction of the jet and b) Number of tracks in the 90° cone around the opposite direction of the jet. The circles are data, the shaded area is the background MC. The dashed line is the predicted signal $Z^0 \to \nu N$ for a mass of 10 GeV. The arrows indicate the position of cuts.

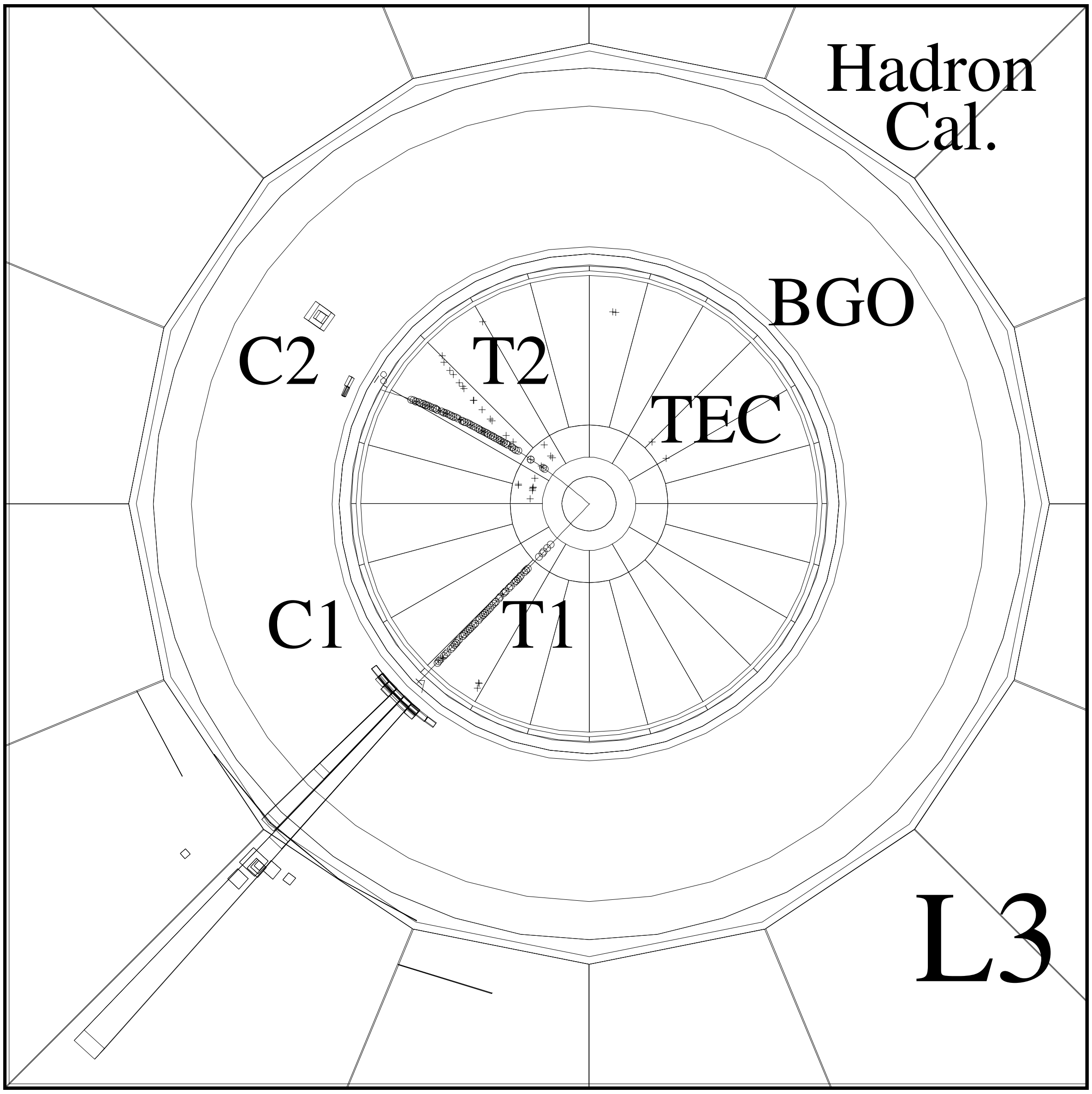

Figure 2: Front view of the monojet candidate event : the event has two electromagnetic clusters and two tracks. The most energetic cluster C1 has an energy 33.4 GeV and the corresponding track T1 has a positive charge and a momentum of 28.3 GeV/c. The second cluster C2 has an energy of 121 MeV and the track T2 has a negative charge and a momentum of 168 MeV. The cluster C1 is compatible with an electron.

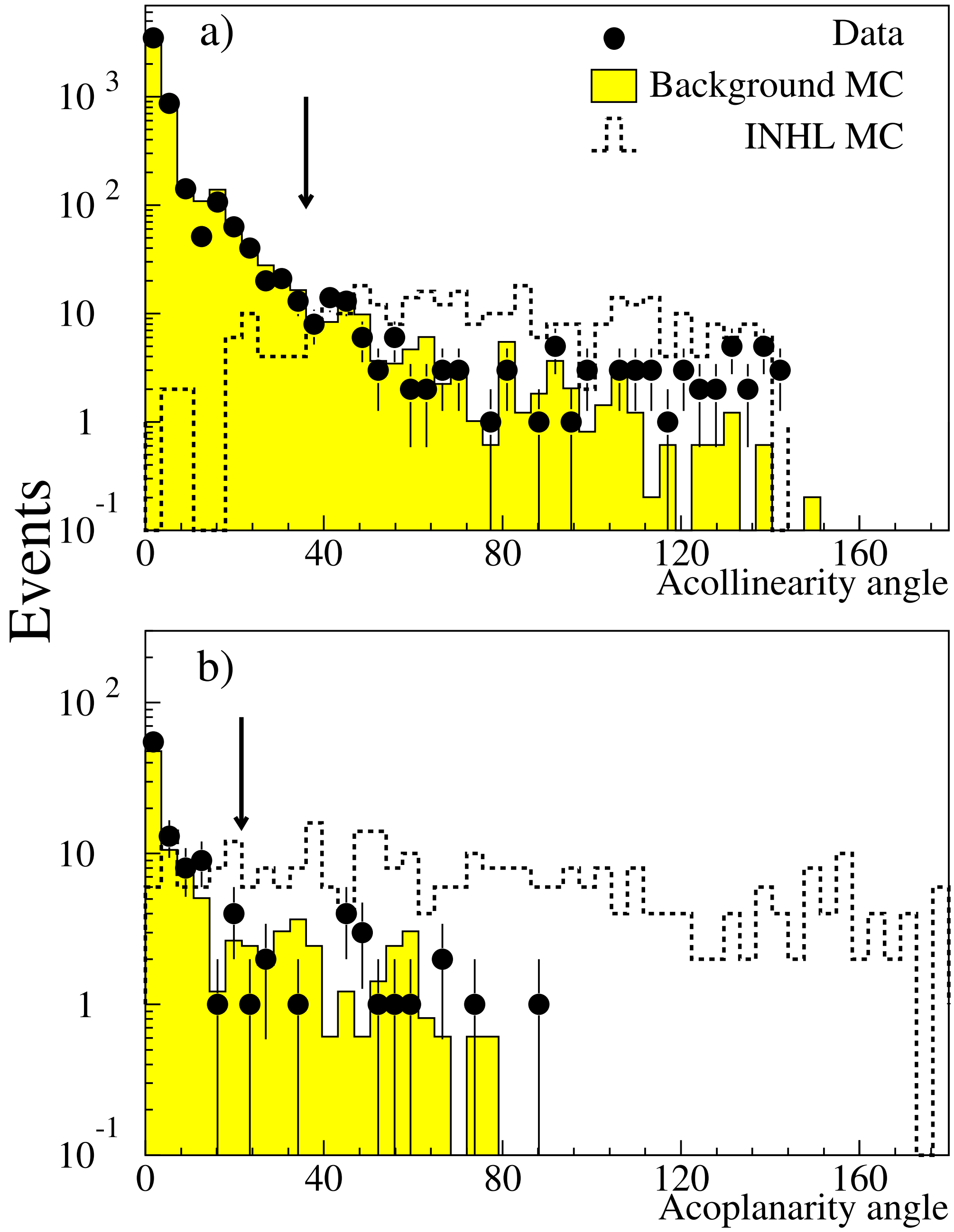

Figure 3: a) Acollinearity η and b) Acoplanarity $\delta\phi$ angle of the two jets. The circles are data, the shaded area is the background MC. The dashed line shows the predicted signal $Z^0 \to \nu N$ for a mass of 50 GeV. The arrows indicate the position of cuts.

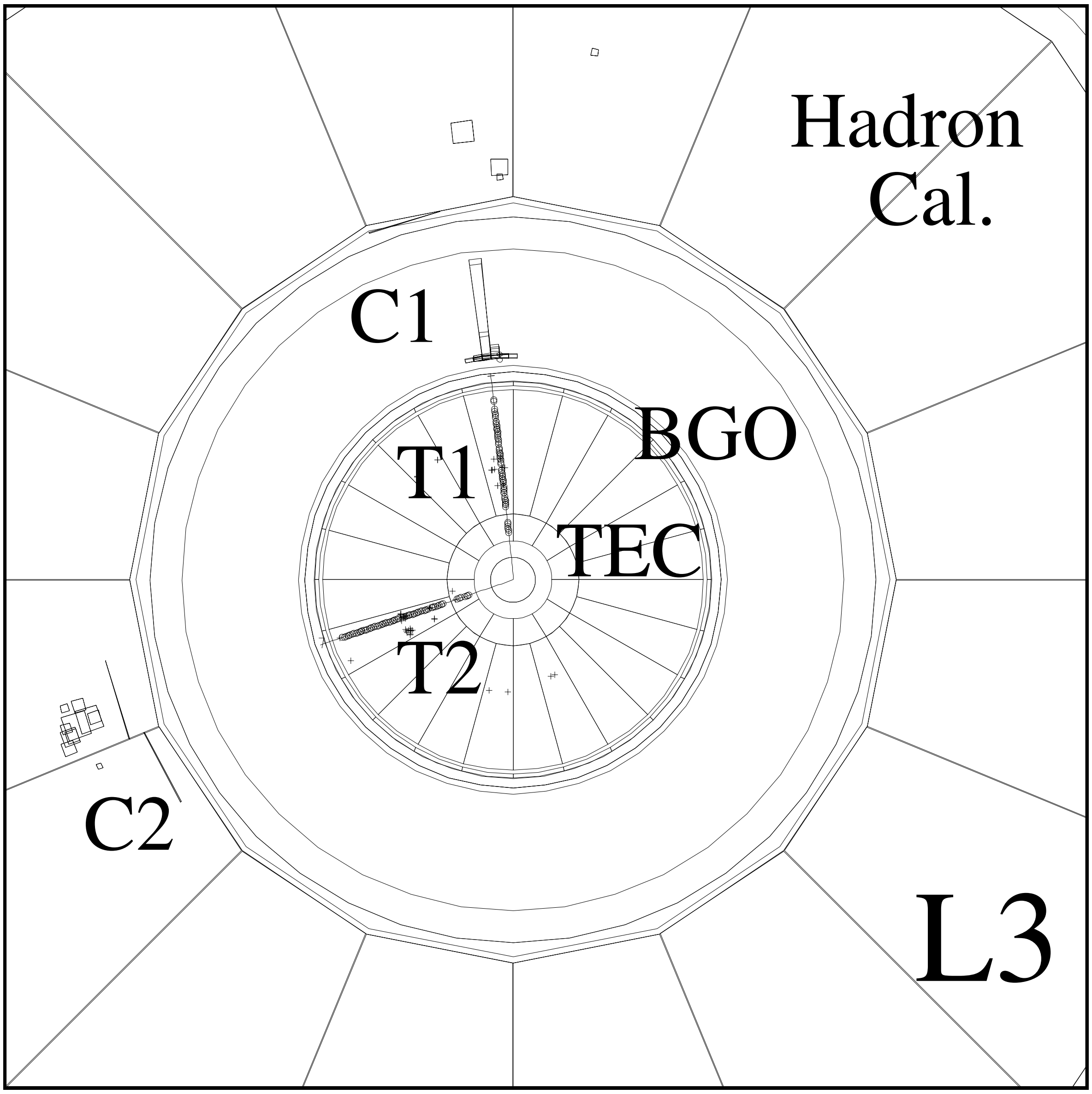

Figure 4: Front view of the two jet candidate: the cluster C1 has an energy of 10.5 GeV and the track T1 has positive charge and a momentum of 5.3 GeV. The cluster C2 has an energy of 5.6 GeV and the track T2 has a negative charge and a momentum of 4.9 GeV. The direction of the missing momentum points into the barrel region.

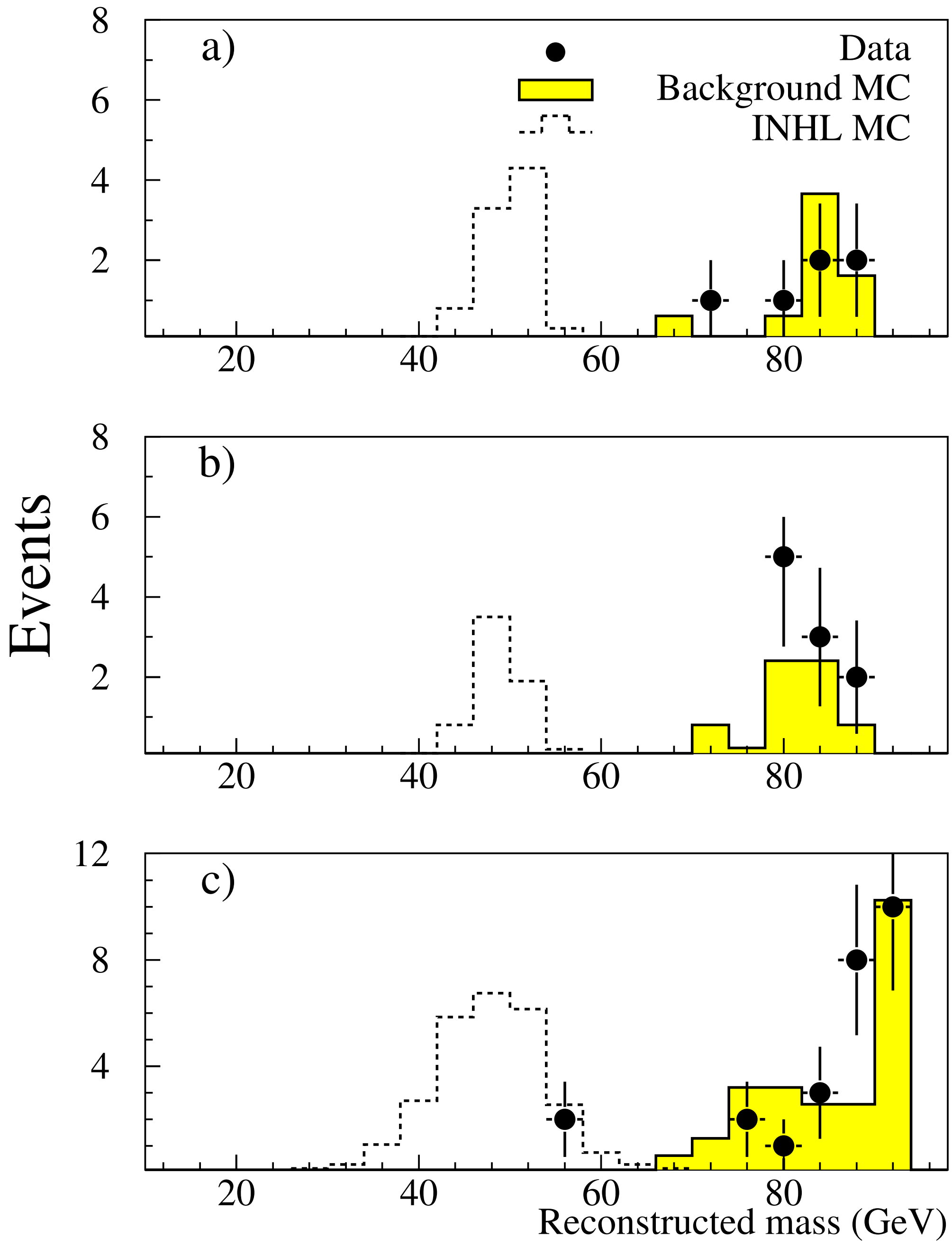

Figure 5: Distribution of invariant mass of the candidate events compatible with a) $\mathrm{N} \rightarrow \mathrm{e q \bar{q}}$, b) $\mathrm{N} \rightarrow \mu \mathrm{q \bar{q}}$ and c) $\mathrm{N} \rightarrow \tau \mathrm{q \bar{q}}$. The circles are data, the shaded area is the background MC. The dashed line shows the predicted signal $\mathrm{Z}^0 \rightarrow \nu N$ for a mass of 50 GeV.

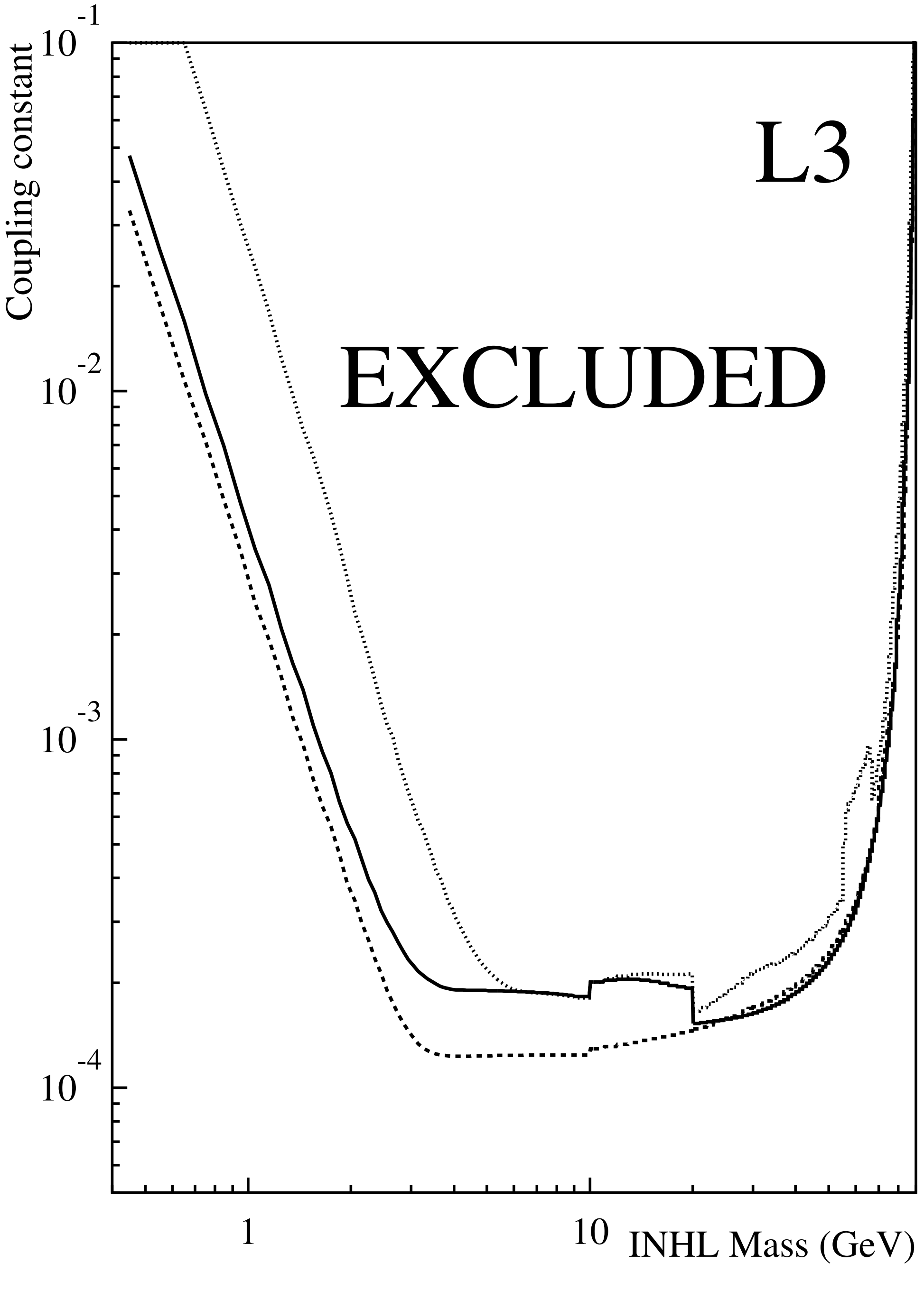

Figure 6: The 95% C.L. upper limit on the coupling constant $|U_\ell|^2$ as a function of the mass of the isosinglet neutral heavy lepton. The solid line is the limit for N_e, the dashed line is the limit for N_μ and the dotted line is for N_τ.

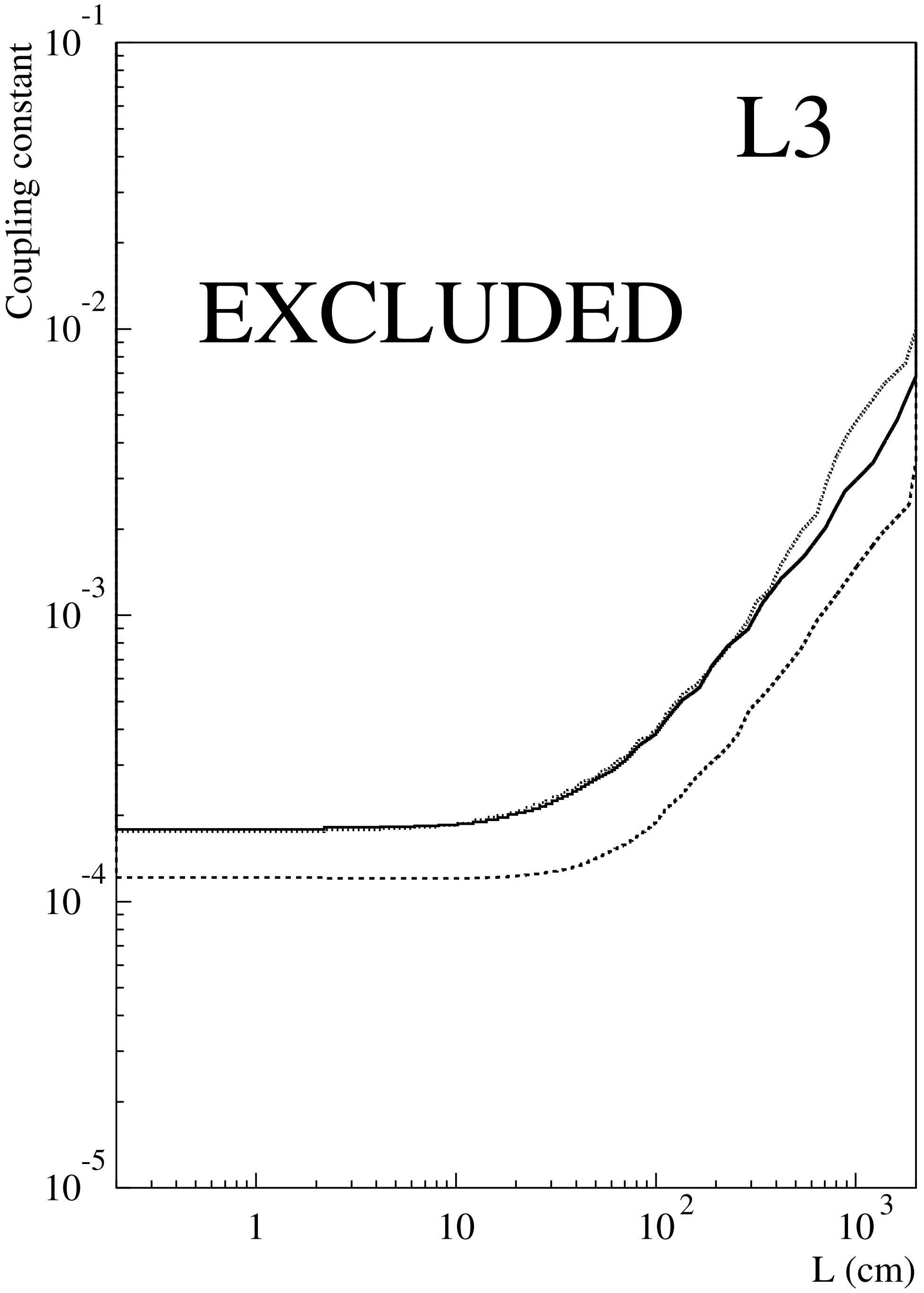

Figure 7: The 95% C.L. upper limit on the coupling constant $\mid U_\ell \mid^2$ as a function of the mean decay length. The solid line is the limit for N_e, the dashed line is the limit for N_μ and the dotted line is for N_τ.